IEEE Access
Multidisciplinary ⋮ Rapid Review ⋮ Open Access Journal

Received 9 April 2025, accepted 12 May 2025, date of publication 16 May 2025, date of current version 23 May 2025.

Digital Object Identifier 10.1109/ACCESS.2025.3570976

RESEARCH ARTICLE

3D-Printed Demultiplexer Circuits Using Suspended-in-Air Grating Couplers for Terahertz Communications

BABAK YAHYAPOUR[1], FRÉDÉRIC MARCOTTE[2], ROYA GACHILOO[1], AND MAKSIM SKOROBOGATIY[1], (Senior Member, IEEE)

[1]Department of Engineering Physics, École Polytechnique de Montréal, Montreal, QC H3T 1J4, Canada
[2]Department of Electrical Engineering, Université Laval, Québec City, QC G1V 0A6, Canada

Corresponding author: Babak Yahyapour (babak.yahyapour@polymtl.ca)

The work of Maksim Skorobogatiy was supported in part by the Natural Sciences and Engineering Research Council of Canada (NSERC) Discovery Grant.

ABSTRACT Integrated photonic circuits are in great demand for the upcoming THz communications. This work explores 3D printing to realize high-quality, high-refractive-index-contrast integrated components and devices for demultiplexing terahertz channels within the Wavelength Division Multiplexing modality. Namely, by printing integrated circuits using Polypropylene filaments suspended in air, we profit from the high-refractive index contrast of such a material combination to realize relatively compact low-loss waveguides, bends, couplers, and fiber Bragg gratings. The two-nozzle FDM printer allows simultaneous printing with filaments of two distinct sizes of 800um and 400um, with the larger filament used to make waveguides and couplers, and the smaller one used to define high-quality fiber Bragg gratings containing as much as 100 periods and featuring stop bands as wide as 10 GHz. Furthermore, by employing judiciously designed mechanical supports we show how to integrate such subcomponents into functional components such as single-channel drop filters. Finally, we developed a low-loss splicing technique for joining several components into functional devices and demonstrated four-channel THz WDM demultiplexers with in-plane (horizontal) and a more compact out-of-plane (vertical) integration. Experimentally, three-channel demultiplexers of THz signals with individual data rates up to 6 Gbps were demonstrated. Using finite element numerical modeling, integrated circuits were optimized for operation in the 120-165 GHz frequency band featuring ∼5 GHz individual channel bandwidths and ∼3 GHz inter-channel spectral spacing, and good agreement with the experiments was observed. Additionally, the measured spectra closely resemble the simulated ones but exhibit a frequency shift of several GHz towards higher frequencies. Experimental results further reveal strong sidelobe suppression and a broader Drop port bandwidth (∼6 GHz vs. ∼4 GHz predicted). However, the measured Drop amplitudes (∼0.5–0.6) are lower than the theoretical predictions (∼0.8) due to ∼10% scattering losses per supporting structure. We believe that the suspended-in-air integrated terahertz circuits hold strong potential for developing various linear optic transformers that will play a key role in energy-efficient analog processing of data streams for the upcoming terahertz communications. This is because of the high quality of the resultant circuits, ease of fabrication, and low infrastructure costs necessary for their manufacturing, thus allowing low-cost fast turnaround prototyping and development of terahertz signal processing devices even with the simplest 3D printing systems.

INDEX TERMS 3D printing, demultiplexer, integrated photonic circuits, wavelength-division multiplexer (WDM).

I. INTRODUCTION

Most wireless systems currently operate in the overcrowded microwave band, which is insufficient to meet the future

The associate editor coordinating the review of this manuscript and approving it for publication was Norbert Herencsar.

© 2025 The Authors. This work is licensed under a Creative Commons Attribution 4.0 License.
For more information, see https://creativecommons.org/licenses/by/4.0/

bandwidth demand. Shifting the carrier wave to higher frequencies is essential to accommodate the anticipated surge in data volume [1], [2]. Consequently, the terahertz (THz) frequency band (0.1-10 THz) is regarded as the next frontier for wireless communication systems [3], [4], [5], [6]. Terahertz (THz) waves situated between microwave and infrared spectral bands attracted much interest for a variety of industrial applications in sensing [7], [8], imaging [9], [10], and security [11], [12] due to their many unique properties. Specifically for communications [3], [4], [13], [14], [15], [16], [17], [18], [19], THz waves enable larger bandwidths than microwaves, potentially enabling several 100 Gbps data rates per channel without any multiplexing. The expected increase in data traffic over the next decade, driven by nascent technologies such as the Internet of Things, Virtual and Augmented Reality, Artificial Intelligence, Big Data, etc. has prompted the development of the sixth generation (6G) wireless networks that greatly surpass existing 4G and 5G network standards.

Terahertz communications is a promising technology for the 6G networks capable of terabit-per-second wireless and fiber-assisted transmission for various data-demanding applications [20], [21], [22], [23], [24], [25], [26], [27]. To date, several demonstrations of free-space ultra-high bit rate data transfer (>100 Gbps) employed single-channel THz links with optical multiplexing [28], [29], [30], as well as advanced modulation techniques including quadrature amplitude modulation and quadrature phase-shift keying [31], [32], [33]. One promising way of data multiplexing in the THz range is Frequency Division Multiplexing (FDM), which encodes different channels using distinct carrier frequencies [34], [35]. A multiplexer (Mux) and a demultiplexer (Demux) are essential components in FDM technology. The multiplexer combines light from spatially separated spectrally distinct sources into a single data stream, while the demultiplexer spatially separates the multiplexed frequencies into single carrier frequency channels [36], [37], [38], [39].

The fabrication of THz devices often involves significant complexity. A standard way uses the methods and infrastructure of silicon photonics to fabricate low-loss THz optical elements [40], [41], [42], [43]. While scalable for mass production, this approach requires access to very expensive infrastructure and entails high running costs, which makes it ill-suitable for rapid prototyping. Alternatively, certain thermoplastics used in additive manufacturing exhibit transparency to terahertz (THz) radiation, which opens an interesting opportunity for 3D printing as a cost-efficient alternative for rapid prototyping of THz devices. As a result, 3D printing has recently gained considerable attention within the Terahertz research community, leading to the development of numerous 3D-printed THz components such as freeform microwave waveguides, antennas, and basic optical elements [44], [45], [46], [47], [48], [49], [50], [51]. Furthermore, 3D printing opens a way for high-density integration of photonic circuits in three dimensions, a feat challenging to accomplish with other methods. For example, Ortiz-Martinez et al. developed a 3D-printed filter made of polystyrene (PS) for the sub-THz 200-300 GHz band [52]. Weidenbach et al. demonstrated 3D-printed waveguide designs, including low-loss splitters and couplers, operating at 120 GHz, fabricated from polystyrene [53]. Additionally, 3D-printed terahertz grating couplers have been designed and characterized at 120 GHz for outcoupling and focusing THz radiation [54]. Furthermore, low-loss, low-dispersion waveguides printed from PS have achieved error-free performance at a data rate of 1 Gb/s [55].

Compared to recent studies, our work presents a novel 3D-printed terahertz demultiplexer featuring suspended-in-air grating couplers, offering significant advantages in fabrication flexibility, cost-effectiveness, and scalability. Unlike the photonic crystal-based demultiplexers proposed by Li et al. [56], which rely on cascaded directional coupling waveguides created by selectively removing rows of silicon rods, our approach eliminates the need for complex lithographic fabrication and precise photonic crystal alignment. Furthermore, while Wu et al. [57] demonstrated a metamaterial-based demultiplexer with high isolation and low insertion loss, its resonance-dependent design requires high precision fabrication and limits both scalability and tunability. In contrast, our 3D-printed demultiplexer circuits allow for customized integration into various THz systems, providing a more adaptable and practical solution for terahertz communication applications. Our presented demultiplexer enables precise, wavelength-specific separation of THz signals while offering significant advantages in terms of fabrication flexibility, cost-effectiveness, and scalability. Our method leverages the versatility of even the basic FDM 3D printing to create complex geometries that are difficult to achieve with conventional techniques, ultimately enhancing signal separation and overall system performance.

In this work, we demonstrate experimentally 3-channel demultiplexers with 2D (in-plane) and 3D (out-of-plane) integration for Frequency Division Multiplexing in the 100-200 GHz spectral band using Side-Coupled Waveguide Bragg Grating Filters as enabling building blocks. The devices were fabricated from a low-loss Polypropylene dielectric using Fused Filament Fabrication (Raise 3D Pro2 series). To the best of our knowledge, this is the first time that devices of such complexity have been realized using 3D printing, in the planar and vertically integrated variants. The advanced optical performance of our demultiplexers stems from the use of polypropylene (PP) polymer in air- a high refractive index contrast material combination that offers one of the lowest absorption losses in the THz regime. However, the 3D printing process introduces several challenges, including warping, adhesion difficulties, and variations in nozzle speed, printed waveguide size, and filament quality, all of which can affect the precision and performance of the printed gratings. To mitigate these limitations and ensure high fabrication accuracy, we have systematically optimized the

printing parameters, effectively minimizing structural deviations (judged from microscopy images) and enhancing the overall reliability of the fabricated demultiplexers (judged by repeatability of the performance from sample to sample).

The paper is organized as follows. First, we discuss the numerical design and optimization of Side-Coupled Waveguide Bragg Grating Filters capable of dropping individual 3 GHz-wide channels with center frequencies in the 140-170 GHz range, while letting other frequencies pass through. Particular attention is paid to the design and fabrication of Waveguide Bragg Gratings [58], [59] which are principal enabling elements of our spectral filters. Then, we discuss the spectral characterization of several such filters using an in-house photonics-based THz communication system [14]. Finally, we show how such filters can be integrated into 3-channel demultiplexers using either in-plane (2D) or out-of-plane (3D) integration strategies and conduct spectral and Bit Error Rate characterization of the resultant devices.

II. DESIGN OF THE WDM THZ FILTERS

Recent advancements in integrated waveguide Bragg grating (WBG) devices have highlighted their potential in microwave and IR for applications such as optical filtering, tunable delays, optical differentiation, and single-sideband modulation. WBG devices offer compactness, flexibility, and high efficiency, making them ideal for applications that require high-performance signal processing. Their ability to operate at THz bandwidths and integrate with other photonic components opens new possibilities for the development of high-speed, low-cost microwave photonic systems [60], [61]. Oh et al. demonstrated a tunable wavelength filter using Bragg gratings in polymer waveguides, leveraging the thermo-optic effect to efficiently shift the Bragg reflection wavelength. This approach achieved a tuning range of over 10 nm with low insertion loss [62].

The Side-Coupled Waveguide Bragg Grating Filter used in our work is an integrated photonic device for filtering out a specific wavelength of light. The schematic of such a device is shown in Fig. 1. (a). The principle of operation of such a device is as follows. The THz light with a mix of wavelengths (e.g. λ_1, λ_2, λ_3) enters the filter through the In port, propagates through a bend, and encounters a waveguide Bragg grating. Wavelengths that fall outside of the grating stopband (e.g. λ_2, λ_3) continue through the grating while being redirected from the top waveguide to the bottom waveguide by the directional coupler, finally exiting the Through port. At the same time, wavelengths falling into the Bragg grating stop band (e.g. λ_1) are reflected by the grating while being redirected from the top waveguide into the bottom waveguide by the directional coupler, finally exiting at the Drop port.

The design process for such a filter involves three main steps: designing the Waveguide Bragg Grating, designing the directional coupler, and optimizing the overall structure. The first step is to design the Waveguide Bragg Grating, which is responsible for dropping a specific wavelength.

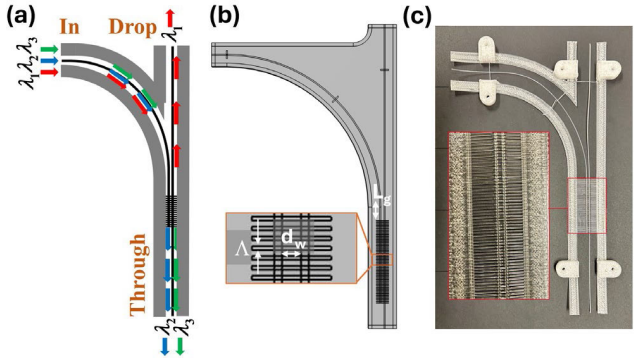

FIGURE 1. (a) A schematic of a WDM demultiplexer (b) A typical computational cell used in numerical simulations. (c) A photo of a WDM demultiplexer. Inset: zoom of a grating section.

This involves selecting a grating period (Λ) based on the desired drop frequency. The period is chosen to ensure that the Bragg grating stop band is centered around one of the channel carrier frequencies (e.g. 140 GHz). The second step involves designing a directional coupler, which includes a circular arc, and two waveguides running directly under the Bragg Grating. First, a separation distance dw between two parallel waveguides is set to result in a relatively short device that can be printed using a 30 cm x 30 cm build plate of a 3D printer. Smaller values of dw result in stronger coupling between two waveguides, and, thus, smaller device size. Next, the number of grating periods Ng is estimated to achieve near-zero transmission for wavelengths within the grating stop band. The exact number of periods in the grating is chosen, so that a second channel outside of the grating stop band (e.g. 145 GHz) is diverted from the launch waveguide into the Through port of a coupler. Finally, the standoff distance between the bend termination and the grating Lg is chosen so that the intensity in the Drop port is maximized at the center frequency of a dropped channel. To perform optimizations, we used finite element COMSOL Multiphysics software with a typical computation cell shown in Fig. 1 (b).

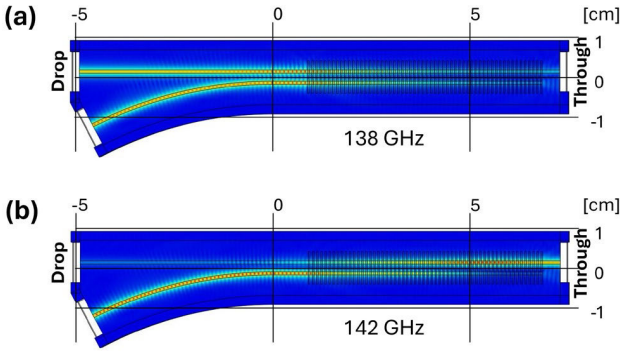

FIGURE 2. Electric field amplitude distribution in the Demux1 operating at (a) Drop (138 GHz) and (b) Through (142 GHz) frequencies.

Three devices were numerically optimized to have Drop channels centered around 138 GHz, 142 GHz, and 146 GHz,

with the Through frequencies ∼4GHz above the Drop channel center frequencies. In Fig 2 electric field amplitude distributions are shown for Demux1 operating at the Drop (138 GHz) (panel a)) and Through (142 GHz) frequencies (panel b)). Drop and Through transmission coefficients (by power) are shown in Fig 4 (a) and (b) (computed using numerical cells shown in Fig. 2). Finally, the geometric parameters of three multiplexers including the grating period, the number of grating periods, the distance between two parallel waveguides, and the standoff distance between the bend termination and the grating are summarized in Table 1.

TABLE 1. Geometrical parameters of three demultiplexers.

Demultiplexer	Demux1	Demux2	Demux3
Drop channel design center frequency (GHz)	138	142	146
Grating period Λ (μm)	1020	984	949
Number of grating periods	57	63	76
Inter-waveguide distance d_w in a coupler (mm)	1.95	1.95	1.95
A standoff distance L_g between the bend termination and the grating (mm)	9	15	21

III. EXPERIMENTAL REALIZATION OF THE WDM THZ FILTERS

The experimental realization of thus designed filters is challenging. The difficulty arises from the need for precise alignment of the waveguide Bragg grating relative to the waveguide coupler and providing mechanical support for the suspended-in-air components of the structure. To this end, the filter components are printed within a rigid hollow frame that features several slender support elements. The first printed layer contains slender support attached to the frame. The second layer contains all the waveguides printed on top of the supports using a 0.8mm diameter nozzle. Finally, the third layer contains Bragg grating printed on top of the waveguide layer using a 0.4 mm diameter nozzle. The grating extends to the support frame for mechanical stability. To splice several filters together a 1mm-diameter glass capillary of 100um wall thickness is used to align and put in contact the Through and In waveguides of the two filters. The capillary is then heated to fuse the plastic waveguides and then removed by shattering. Finally, the device is assembled on the optical bench with the frame kept under light tension using alignment screws. A photo of a typical demultiplexer is shown in Fig. 1 (c).

IV. OPTICAL CHARACTERIZATION OF THE WDM THZ FILTERS

Optical characterization of the 3D-printed demultiplexers was conducted using an in-house photonics-based THz communication system detailed earlier [46]. The schematic of the optical characterization setup is presented in Fig. 3(a), while Fig. 3(c) shows a photo of the measurement setup with a mounted device. Briefly, in the transmitter arm, two DFB lasers, independently tunable and operating within the infrared C-band with somewhat mismatched center frequencies, are combined using a 3 dB coupler and sent to a fiber-coupled photomixer to generate THz waves of fixed frequency anywhere in the ∼0.1-1 THz range with bandwidth of ∼10MHz. In the THz CW spectroscopy mode: the THz radiation of a set frequency from the photomixer (Model: IOD-PMD-14001 from NTT Electronics Inc) is guided through a WR-6 rectangular waveguide flange [see Fig. 3(a)], which is butt-coupled to the device under study. On the receiving end, a 10.8 mm diameter horn antenna collects the THz waves, which are then detected using a zero-bias Schottky detector (Model: WR8.0 ZBD-F from Virginia Diodes Inc). A high-gain, low-noise amplifier (Model: SLNA-030-32-30-SMA from Fairview Microwave Inc) is then used to amplify the received signal for further processing. In the THz communication mode [see Fig. 3 (b)]: a baseband signal source, generated by a pulse pattern generator integrated into the test equipment, produces pseudorandom bit sequences with varying bit rates. This signal undergoes amplification and modulation utilizing RF and Mach-Zhender modulation techniques. The modulated laser beams are further amplified and injected into a photomixer to generate a modulated THz carrier wave. In the receiver section, the THz carrier wave is detected and demodulated using a zero-bias Schottky diode, then amplified through a low-noise amplifier. Eye pattern and bit error rate (BER) are then recorded. In more details, at the emitter side, the combined infrared optical signal from the coupler is modulated using an external electro-optic modulator (Models: LN81S-FC and MX10A from Thorlabs Inc). The modulated optical signal, with a fixed output power, is then amplified using an Erbium-Doped Fiber Amplifier (EDFA). At the receiver side, a Bias-Tee filters the DC field from the demodulated baseband signal, and a low-noise amplifier (LNA) further amplifies the received signal. Finally, the demodulated baseband signals are analyzed using a high-speed oscilloscope and a BER tester (Model: MP2100B from Anritsu Corporation). The BER measurements were conducted by varying the bit rate from 1 Gbps to 6 Gbps or adjusting the carrier frequency at a fixed bit rate. At each bit rate or carrier frequency, the decision threshold was optimized to balance insertion errors (digital zero misidentified as one) and omission errors (digital one misidentified as zero), thereby minimizing the BER.

In the experiments, the THz carrier wave in the 120 – 165 GHz spectral range was generated using an

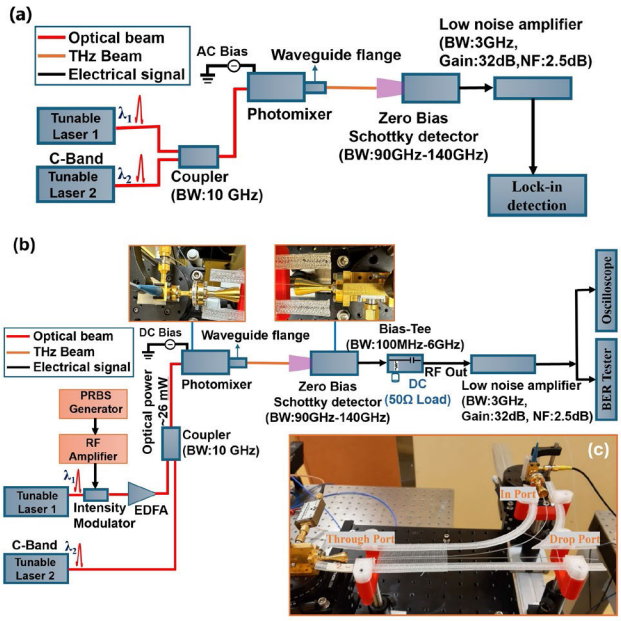

FIGURE 3. **(a) Schematic of the continuous wave THz spectroscopy system. (b) Schematic of the photonics-based THz communication system. (c) Photo of the measurement setup with a mounted device.**

optical photomixer (IOD-PMD-14001, NTT Electronics) with a photocurrent of 7mA generating THz powers between 125 μW (-9 dBm) and 250 μW (-6 dBm), and then coupled into a demultiplexer via a 1-inch-long WR6.5 rectangular waveguide terminated with a horn (WR8.0 ZBD-F, Virginia Diodes). A similar configuration was utilized at the output port of a demultiplexer where a horn was connected via a 1-inch-long WR6.5 rectangular waveguide to the Schottky diode. Operation of the Drop and Through ports of the filters were then characterized using two complimentary measurement modes, namely, THz CW spectroscopy and BER characterization for data transmission.

First, CW THz spectroscopy was conducted on three demultiplexers without data modulation. To extract the relative Drop and Trough coefficients (shown in Figs. 4(c,d)) for direct comparison with theoretical predictions (computed using numerical cells shown in Fig. 2) we normalize the raw transmission data by the transmission of a stand-alone bent waveguide (R_b =10 cm, 90°-bend) identical to those used in the filters (see insert in Fig. 4(c)). We note that overall, numerically computed spectra (shown in Figs. 4(a,b)) have very similar shapes to the measured ones. Additionally, as per the design goal, the higher-frequency edge of the Trough spectra shows higher transmission than the lower-frequency edge. At the same time, the experimental spectra are shifted to higher frequencies by several GHz. Moreover, we observe strong sidelobe suppression outside of the stopband in experimental spectra which results in the ~6 GHz experimental bandwidths at the Drop port, which is somewhat larger than numerically predicted bandwidths of ~4 GHz. Finally, the maximal amplitudes of the measured Drop spectra are somewhat lower (~0.5-0.6) compared to the theoretical ones (~0.8), due to scattering losses on supporting structures (10% scattering loss per structure predicted numerically using numerical cell shown in Fig. 1(b)), as well as due to nonuniformities of 3D-printed waveguides including wall roughness and micro-bending. The overall insertion loss is estimated to be 1.7 dB for the Drop port, and 1 dB for the Through port, which implies that with even a modest power budget of 11 dB, one can build a 10-channel THz WDM system using such filters placed in sequence.

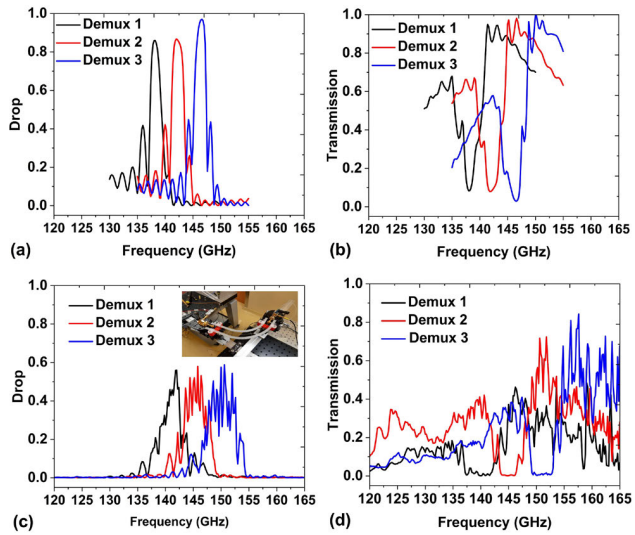

FIGURE 4. **(a) Drop and (b) Through spectra as predicted by numerical simulations. Relative (c) Drop and (d) Through coefficients when using transmission through a stand-alone bend as a reference. Insert: picture of a stand-alone waveguide bend.**

Next, we characterize information transmission through the 3 thus-developed multiplexors. Using Fig. 4, we chose the channel center frequencies as follows: demultiplexer 1 (Drop 140 GHz, Through 145 GHz), demultiplexer 2 (Drop 145 GHz, Through 150 GHz), and demultiplexer 3 (Drop 150 GHz, Through 155 GHz). Therefore, all the following BER measurements will be conducted at those frequencies. Specifically, the eye patterns for the THz data streams of various bit rates ranging from 1 to 6 Gbps using amplitude-shift-keying modulation were recorded, and corresponding Bit Error Rate (BER) measurements were conducted. During BER measurements, the decision threshold was adjusted to balance the insertion error (incorrectly identifying a digital 0 as a digital 1) and omission error (incorrectly identifying a digital 1 as a digital 0). The duration of recording was determined as 1/(target BER $\times$ bit rate), with the target BER set to 10^{-12} (error-free transmission threshold). First, the performance of Demux1 was characterized in the Drop mode at the carrier frequency corresponding to the grating stopband center frequency of 140 GHz. Next, the performance of Demux1 was characterized in the Through mode using the carrier outside of the grating stopband at 145 GHz as shown in Fig. 5(a). Similarly, performances of Demux2 and Demux3

were characterized in Drop mode at the corresponding stopband center frequencies of 145 GHz and 150 GHz, as well as in Through mode outside of the corresponding stopbands at 150 GHz and 155 GHz as shown in Figs. 5(b,c). Experimental data confirms that all demultiplexers can operate with 6Gbps data streams with BER$<10^{-4}$ below the forward error correction limit of $\sim 10^{-3}$.

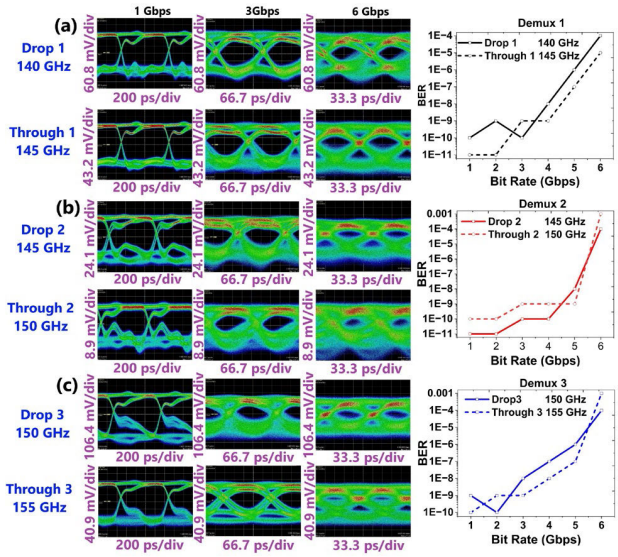

FIGURE 5. Measured Bit Error Rate (BER) versus Bit Rate in the 1-6 GBps range and the corresponding eye diagrams for 3 demultiplexers (a) Demux1 (b) Demux2, and (c) Demux3 at the Drop and Through ports.

V. WDM DEVICES – TWO DEMULTIPLEXERS CONNECTED IN SEQUENCE

In the following, we demonstrate 3-channel demultiplexers using two filters from the previous section connected in sequence (schematically shown in Fig. 6(a)). The first device was made by splicing the Through 1 and In 2 ports of Demux 1 and Demux 2 (Demux 1+2), while the second one was made by splicing the Through 2 and In 3 ports of Demux 2 with Demux 3 (Demux 2+3) as shown in Fig. 6(b). Then, spectroscopic and BER measurements were performed at various Drop and Through ports.

Fig. 7 (a) shows the Drop 1 spectrum, while Fig. 7 (b) shows Drop 2/Through 2 spectra in the range of 120–165 GHz for Demux 1+2. Similarly, Fig. 7 (c) shows the Drop 2 spectrum, while Fig. 8 (d) shows Drop 3 and Through 3 spectra for Demux 1+3.

The communication performance of in-sequence demultiplexers was evaluated by measuring the bit error rate (BER) while adjusting the bit rate from 1 to 6 Gbps. Specifically, for Demux 1+2, BER was measured at 140 GHz for the Drop 1 port, 145 GHz for the Drop 2, and 150 GHz for the Through 2 ports. The measured bit error rate (BER) versus bit rate, along with the corresponding eye diagrams for Demux 1+2 are shown in Figure 8 (a-d). Similarly, for Demux 2+3 BER was measured at 145 GHz for the Drop 1 port, 150 GHz

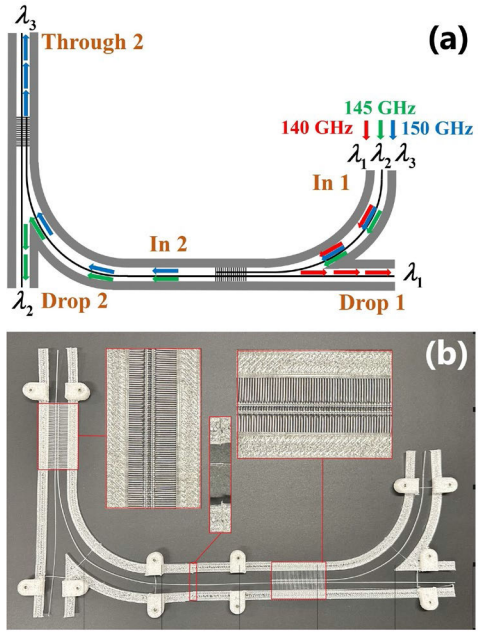

FIGURE 6. (a) A schematic of the in-sequence demultiplexer (Demux 1+2). (b) A photo of the assembled device.

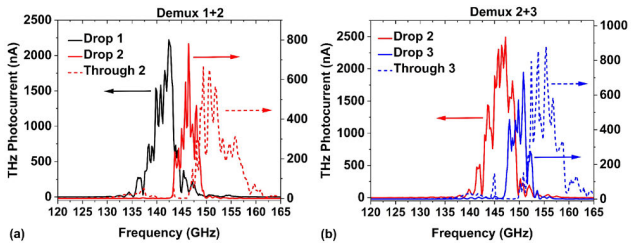

FIGURE 7. Experimental spectra of (a) Drop 1, (b) Drop 2, and Through 2 of the Demux 1+2. Experimental spectra of (c) Drop 2, (d) Drop 3, and Through 3 of the Demux 2+3.

for the Drop 3 port, and 155 GHz for the Through 3 port. The measured BER versus bit rate, along with the corresponding eye diagrams, are presented in Figure 8 (d-h).

VI. WDM DEVICES – TWO DEMULTIPLEXERS CONNECTED IN PARALLEL

Finally, we demonstrate 3-channel demultiplexers using two filters connected in parallel (schematically shown in Fig. 9(a)). The first device was made by splicing the In and Through ports of Demux 1 and Demux 2 (Demux 1||2), while the second one was made by splicing the In and Through ports of Demux 2 with Demux 3 (Demux 2||3) as shown in Fig. 9(b). Then, spectroscopic and BER measurements were performed at various Drop and Through ports.

Experimental spectra at the Drop 1, Drop 2, and Through 1+2 ports of the in-parallel Demux 1||2 are shown in Fig. 10 (a) in the spectral range of 120–165 GHz. Similarly, experimental spectra at the Drop 2, Drop 3, and Through 2+3 ports of the in-parallel Demux 2||3 are shown in Fig. 10 (b).

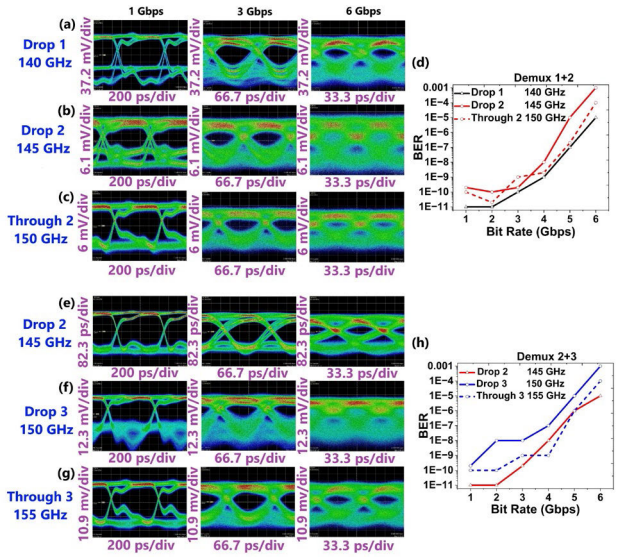

FIGURE 8. Measured Bit Error Rate versus Bit Rate and the corresponding eye diagrams for in-sequence Demux 1+2 at different bitrates (a) eye pattern at the Drop 1 port (b) eye pattern at the Drop 2 port (c) eye pattern at the Through 2 port (d) BER at the Drop 1, Drop 2, and Through 2 ports. Similar data is shown in panels (e)-(h) for Demux 2+3 and ports Drop 2, Drop 3, and Through 3 ports.

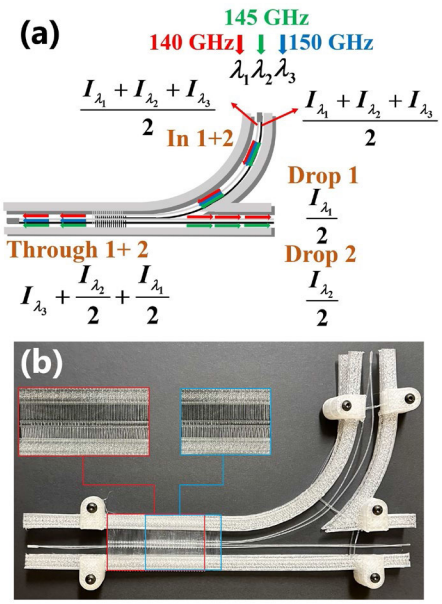

FIGURE 9. (a) A schematic of the in-parallel demultiplexer (Demux 1||2). (b) A photo of the assembled device.

The communication performance of the in-parallel Demux 1||2 was evaluated by measuring the bit error rate (BER) for bit rates between 1 and 6 Gbps. Specifically, BER was measured at 140 GHz for Drop 1, 145 GHz for Drop 2, and 140 GHz, 145 GHz, and 150 GHz for the composite Through 1+2 ports. The measured bit error rate (BER) versus bit rate, along with the corresponding eye diagrams for the Demux 2|3 are shown in Figs. 11 (a-d). Similarly, for Demux 2|3

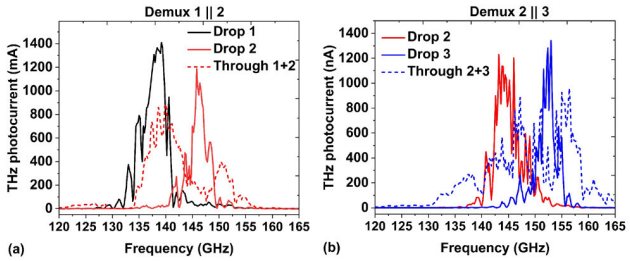

FIGURE 10. (a) Experimental Drop 1, Drop 2, and through 1+2 spectra of the Demux 1||2. (b) Experimental Drop 2, Drop 3, and through 2+3 spectra of the Demux 2||3.

BER was measured at 145 GHz for Drop 1, 150 GHz for Drop 3, and 145 GHz, 150 GHz, and 155 GHz for Through 2+3 ports. The measured BER versus bit rate, along with the corresponding eye diagrams, are presented in Figs. 11 (e-h).

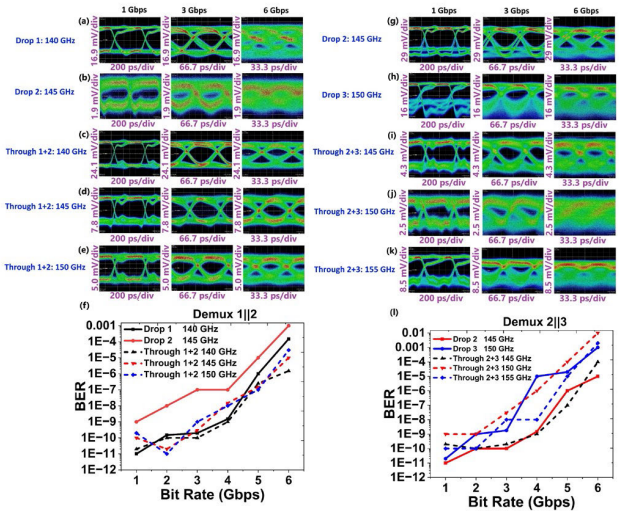

FIGURE 11. Measured bit error rate versus bit rate and the corresponding eye diagrams for in-parallel Demux 1||2 at different bitrates. Eye patterns at the (a) Drop 1 port, (b) Drop 2 port, (c,d,e) through 1+2 port. (e) BER at the Drop 1, Drop 2, and through 1+2 ports. Similar data is shown in panels (g)-(l) for Demux 2||3 and ports Drop 2, Drop 3, and through 2+3.

VII. CONCLUSION

In this work, three THz demultiplexer filters, as well as their combinations in sequence and in parallel were fabricated and characterized for operation with four sub-mm wave channels (140 GHz, 145 GHz, 150 GHz, and 155 GHz) within the WDM framework of Terahertz Communication. Successful channel demultiplexing of 3 channels per device was demonstrated with up to 6Gbps data rates. Experimental results further demonstrate strong sidelobe suppression and a broader Drop port bandwidth (∼6 GHz compared to the predicted ∼4 GHz). However, the measured Drop amplitudes (∼0.5–0.6) are lower than the theoretical predictions (∼0.8), primarily due to approximately 10% scattering losses per supporting structure. Our study indicates that additive manufacturing of THz circuits with a

high-refractive-index-contrast Polypropylene-in-air material combination presents a viable approach for high-quality low-loss fabrication of integrated THz devices. Additionally, additive manufacturing carries a strong potential for three-dimensional integration of THz circuits, as well as a fast turn-around between design and prototyping.

REFERENCES

[1] Y. Niu, Y. Li, D. Jin, L. Su, and A. V. Vasilakos, "A survey of millimeter wave communications (mmWave) for 5G: Opportunities and challenges," *Wireless Netw.*, vol. 21, no. 8, pp. 2657–2676, Nov. 2015.

[2] J. Zhang, P. Tang, L. Tian, Z. Hu, T. Wang, and H. Wang, "6–100 GHz research progress and challenges from a channel perspective for fifth generation (5G) and future wireless communication," *Sci. China Inf. Sci.*, vol. 60, no. 8, Aug. 2017, Art. no. 080301.

[3] I. F. Akyildiz, J. M. Jornet, and C. Han, "Terahertz band: Next frontier for wireless communications," *Phys. Commun.*, vol. 12, pp. 16–32, Sep. 2014.

[4] T. Kleine-Ostmann and T. Nagatsuma, "A review on terahertz communications research," *J. Infr., Millim., THz Waves*, vol. 32, no. 2, pp. 143–171, Feb. 2011.

[5] S. Dang, O. Amin, B. Shihada, and M.-S. Alouini, "From a human-centric perspective: What might 6G be?" *Authorea Preprints*, 2023. [Online]. Available: https://arxiv.org/pdf/1906.00741.pdf

[6] T. Nagatsuma, G. Ducournau, and C. C. Renaud, "Advances in terahertz communications accelerated by photonics," *Nature Photon.*, vol. 10, no. 6, pp. 371–379, Jun. 2016, doi: 10.1038/nphoton.2016.65.

[7] M. Poulin, S. Giannacopoulos, and M. Skorobogatiy, "Surface wave enhanced sensing in the terahertz spectral range: Modalities, materials, and perspectives," *Sensors*, vol. 19, no. 24, p. 5505, Dec. 2019.

[8] Y. Cao, K. Nallappan, H. Guerboukha, T. Gervais, and M. Skorobogatiy, "Additive manufacturing of resonant fluidic sensors based on photonic bandgap waveguides for terahertz applications," *Opt. Exp.*, vol. 27, no. 20, p. 27663, Sep. 2019.

[9] K. Fukunaga, N. Sekine, I. Hosako, N. Oda, H. Yoneyama, and T. Sudoh, "Real-time terahertz imaging for art conservation science," *J. Eur. Opt. Society-Rapid Publications*, vol. 3, p. 8027, Jan. 2008.

[10] H. Guerboukha, K. Nallappan, and M. Skorobogatiy, "Toward real-time terahertz imaging," *Adv. Opt. Photon.*, vol. 10, no. 4, p. 843, Dec. 2018.

[11] Y. C. Shen, T. Lo, P. F. Taday, B. E. Cole, W. R. Tribe, and M. C. Kemp, "Detection and identification of explosives using terahertz pulsed spectroscopic imaging," *Appl. Phys. Lett.*, vol. 86, no. 24, pp. 241116-1–241116-3, Jun. 2005. [Online]. Available: https://doi.org/10.1063/1.1946192

[12] J. F. Federici, B. Schulkin, F. Huang, D. Gary, R. Barat, F. Oliveira, and D. Zimdars, "THz imaging and sensing for security applications—Explosives, weapons and drugs," *Semicond. Sci. Technol.*, vol. 20, no. 7, pp. S266–S280, Jul. 2005.

[13] M. A. Akkaş, "Terahertz wireless data communication," *Wireless Netw.*, vol. 25, no. 1, pp. 145–155, Jan. 2019.

[14] K. Nallappan, H. Guerboukha, C. Nerguizian, and M. Skorobogatiy, "Live streaming of uncompressed HD and 4K videos using terahertz wireless links," *IEEE Access*, vol. 6, pp. 58030–58042, 2018.

[15] S. Koenig, D. Lopez-Diaz, J. Antes, F. Boes, R. Henneberger, A. Leuther, A. Tessmann, R. Schmogrow, D. Hillerkuss, R. Palmer, T. Zwick, C. Koos, W. Freude, O. Ambacher, J. Leuthold, and I. Kallfass, "Wireless sub-THz communication system with high data rate," *Nature Photon.*, vol. 7, no. 12, pp. 977–981, Dec. 2013.

[16] H. Elayan, O. Amin, B. Shihada, R. M. Shubair, and M.-S. Alouini, "Terahertz band: The last piece of RF spectrum puzzle for communication systems," *IEEE Open J. Commun. Soc.*, vol. 1, pp. 1–32, 2020.

[17] H. Li, S. Duan, C. Zheng, J. Li, H. Xu, C. Song, F. Yang, Y. Liu, W. Shi, Y. Zhang, Y. Shen, and J. Yao, "Longitudinal manipulation of scalar to vector vortex beams evolution empowered by all-silicon metasurfaces," *Adv. Opt. Mater.*, vol. 11, no. 22, Nov. 2023, Art. no. 2301368.

[18] H. Li, C. Zheng, S. Duan, J. Li, H. Xu, Y. Li, C. Song, F. Yang, Z. Yue, W. Shi, Y. Zhang, Y. Shen, and J. Yao, "Polarization detection of terahertz waves using all-silicon metasurfaces with tightly focusing behavior," *Laser Photon. Rev.*, vol. 17, no. 12, Dec. 2023, Art. no. 2300428.

[19] H. Li, C. Zhao, J. Li, C. Zheng, H. Xu, W. Xu, Q. Tan, C. Song, Y. Shen, and J. Yao, "Broadband all-dielectric meta-lenses with terahertz full-Stokes polarization detection behavior," *Opt. Exp.*, vol. 32, no. 21, p. 37916, Oct. 2024.

[20] A. Shafie, N. Yang, C. Han, J. M. Jornet, M. Juntti, and T. Kürner, "Terahertz communications for 6G and beyond wireless networks: Challenges, key advancements, and opportunities," *IEEE Netw.*, vol. 37, no. 3, pp. 162–169, May/Jun. 2023.

[21] V. Petrov, T. Kurner, and I. Hosako, "IEEE 802.15.3d: First standardization efforts for sub-terahertz band communications toward 6G," *IEEE Commun. Mag.*, vol. 58, no. 11, pp. 28–33, Nov. 2020.

[22] M. Polese, J. M. Jornet, T. Melodia, and M. Zorzi, "Toward end-to-end, full-stack 6G terahertz networks," *IEEE Commun. Mag.*, vol. 58, no. 11, pp. 48–54, Nov. 2020.

[23] M. Giordani, M. Polese, M. Mezzavilla, S. Rangan, and M. Zorzi, "Toward 6G networks: Use cases and technologies," *IEEE Commun. Mag.*, vol. 58, no. 3, pp. 55–61, Mar. 2020.

[24] L. John, A. Tessmann, A. Leuther, P. Neininger, T. Merkle, and T. Zwick, "Broadband 300-GHz power amplifier MMICs in InGaAs mHEMT technology," *IEEE Trans. TTHz Sci. Technol.*, vol. 10, no. 3, pp. 309–320, May 2020.

[25] J. Kießling, I. Breunig, P. G. Schunemann, K. Buse, and K. L. Vodopyanov, "High power and spectral purity continuous-wave photonic THz source tunable from 1 to 4.5 THz for nonlinear molecular spectroscopy," *New J. Phys.*, vol. 15, no. 10, 2013, Art. no. 105014, doi: 10.1088/1367-2630/15/10/105014.

[26] T. Nagatsuma, M. Sonoda, T. Higashimoto, R. Kimura, L. Yi, and H. Ito, "300-GHz-band wireless communication using Fermi-level managed barrier diode receiver," in *IEEE MTT-S Int. Microw. Symp. Dig.*, Jun. 2019, pp. 762–765.

[27] J. Kiessling, I. Breunig, P. G. Schunemann, K. Buse, and K. L. Vodopyanov, "High power and spectral purity continuous-wave photonic THz source tunable from 1 to 4.5 THz for nonlinear molecular spectroscopy," *New J. Phys.*, vol. 15, no. 10, Oct. 2013, Art. no. 105014.

[28] N. Oshima, K. Hashimoto, S. Suzuki, and M. Asada, "Terahertz wireless data transmission with frequency and polarization division multiplexing using resonant-tunneling-diode oscillators," *IEEE Trans. THz Sci. Technol.*, vol. 7, no. 5, pp. 593–598, Sep. 2017.

[29] H. Zhao, B. Quan, X. Wang, C. Gu, J. Li, and Y. Zhang, "Demonstration of orbital angular momentum multiplexing and demultiplexing based on a metasurface in the terahertz band," *ACS Photon.*, vol. 5, no. 5, pp. 1726–1732, May 2018.

[30] Q. Wang, X. Zhang, E. Plum, Q. Xu, M. Wei, Y. Xu, H. Zhang, Y. Liao, J. Gu, J. Han, and W. Zhang, "Polarization and frequency multiplexed terahertz meta-holography," *Adv. Opt. Mater.*, vol. 5, no. 14, Jun. 2017, Art. no. 1700277.

[31] S. Jia, X. Pang, O. Ozolins, X. Yu, H. Hu, J. Yu, P. Guan, F. Da Ros, S. Popov, G. Jacobsen, M. Galili, T. Morioka, D. Zibar, and L. K. Oxenløwe, "0.4 THz photonic-wireless link with 106 Gb/s single channel bitrate," *J. Lightw. Technol.*, vol. 36, no. 2, pp. 610–616, Jan. 2018.

[32] D. K. Gayen, "Optical multiplexer," *J. Mech. Cont. Math. Sci.*, vol. 18, no. 3, pp. 32–43, Mar. 2023.

[33] K. Liu, S. Jia, S. Wang, X. Pang, W. Li, S. Zheng, H. Chi, X. Jin, X. Zhang, and X. Yu, "100 Gbit/s THz photonic wireless transmission in the 350-GHz band with extended reach," *IEEE Photon. Technol. Lett.*, vol. 30, no. 11, pp. 1064–1067, Jun. 2018.

[34] D. K. Gayen, "Optical multiplexer," *J. Mech. Cont. Math. Sci*, vol. 18, no. 3, pp. 32–42, 2023.

[35] W. Deng, L. Chen, H. Zhang, S. Wang, Z. Lu, S. Liu, Z. Yang, Z. Wang, S. Yuan, Y. Wang, R. Wang, Y. Yu, X. Wu, X. Yu, and X. Zhang, "On-chip polarization- and frequency-division demultiplexing for multidimensional terahertz communication," *Laser Photon. Rev.*, vol. 16, no. 10, Oct. 2022, Art. no. 2200136.

[36] N. Joshi and N. P. Pathak, "Tunable wavelength demultiplexer using modified graphene plasmonic split ring resonators for terahertz communication," *Photon. Nanostruct. Fundam. Appl.*, vol. 28, pp. 1–5, Feb. 2018.

[37] U. Fischer, S. Höll, M. Haupt, and M. Joncic, "Polymeric demultiplexer component for wavelength division multiplex communication systems using polymer fibers," *Proc. SPIE*, vol. 9368, pp. 167–177, Apr. 2015.

[38] M. Haupt and U. Fischer, "Optical design of a low-loss demultiplexer for optical communication systems in the visible range," *Proc. SPIE*, vol. 8550, Dec. 2012, Art. no. 85500J.

[39] M. S. Borella, J. P. Jue, D. Banerjee, B. Ramamurthy, and B. Mukherjee, "Optical components for WDM lightwave networks," *Proc. IEEE*, vol. 85, no. 8, pp. 1274–1307, 1997.

[40] L. Smith, V. Shiran, W. Gomaa, and T. Darcie, "Characterization of a split-ring-resonator-loaded transmission line at terahertz frequencies," *Opt. Exp.*, vol. 29, no. 15, p. 23282, Jul. 2021.
[41] F. Ma et al., "Tunable multiband terahertz metamaterials using a reconfigurable electric split-ring resonator array," *Light Sci. Appl.*, vol. 3, 2014, Art. no. e171. [Online]. Available: https://doi.org/10.1038/lsa.2014.52
[42] G.-B. Wu et al., "3-D-printed terahertz metalenses for next-generation communication and imaging applications," *Proc. IEEE*, vol. 112, no. 8, pp. 1033–1050, Aug. 2024, doi: 10.1109/JPROC.2024.3395891.
[43] F. Ma, Y.-S. Lin, X. Zhang, and C. Lee, "Tunable multiband terahertz metamaterials using a reconfigurable electric split-ring resonator array," *Light, Sci. Appl.*, vol. 3, no. 5, p. e171, May 2014.
[44] G.-B. Wu, J. Chen, C. Yang, K. F. Chan, M. K. Chen, D. P. Tsai, and C. H. Chan, "3-D-printed terahertz metalenses for next-generation communication and imaging applications," *Proc. IEEE*, vol. 112, no. 8, pp. 1033–1050, Aug. 2024.
[45] F.-S. Hsiao, P.-C. Wang, W.-Y. Lin, J.-H. Yan, P. Torkaman, K.-M. Feng, and S.-H. Yang, "A 5G/terahertz integrated wireless network based on wavelength-division multiplexing and terahertz photomixing," in *Proc. 46th Int. Conf. Infr., Millim. THz Waves (IRMMW-THz)*, Aug. 2021, pp. 1–2.
[46] J. Chen, X. Liu, Y. Tian, W. Zhu, C. Yan, Y. Shi, L. B. Kong, H. J. Qi, and K. Zhou, "3D Printed anisotropic polymer materials for functional applications," *Adv. Mater.*, vol. 34, no. 5, 2022, Art. no. 2102877.
[47] H. Xin and M. Liang, "3-D-printed microwave and THz devices using polymer jetting techniques," *Proc. IEEE*, vol. 105, no. 4, pp. 737–755, Apr. 2017.
[48] J. Chen, X. Liu, Y. Tian, W. Zhu, C. Yan, Y. Shi, L. B. Kong, H. J. Qi, and K. Zhou, "3D-printed anisotropic polymer materials for functional applications," *Adv. Mater.*, vol. 34, no. 5, Feb. 2022, Art. no. 2102877.
[49] Y. Cao, K. Nallappan, G. Xu, and M. Skorobogatiy, "Add drop multiplexers for terahertz communications using two-wire waveguide-based plasmonic circuits," *Nature Commun.*, vol. 13, no. 1, p. 4090, Jul. 2022.
[50] Y. Cao, K. Nallappan, H. Guerboukha, G. Xu, and M. Skorobogatiy, "Additive manufacturing of highly reconfigurable plasmonic circuits for terahertz communications," *Optica*, vol. 7, no. 9, p. 1112, Sep. 2020.
[51] J. Li, K. Nallappan, H. Guerboukha, and M. Skorobogatiy, "3D printed hollow core terahertz Bragg waveguides with defect layers for surface sensing applications," *Opt. Exp.*, vol. 25, no. 4, p. 4126, Feb. 2017.
[52] M. Ortiz-Martinez, E. Castro-Camus, and A. I. Hernandez-Serrano, "Guided-mode filters for terahertz frequencies fabricated by 3D printing," *J. Infr., Millim., THz Waves*, vol. 40, no. 7, pp. 731–737, Jul. 2019.
[53] M. Weidenbach, D. Jahn, A. Rehn, S. F. Busch, F. Beltrán-Mejía, J. C. Balzer, and M. Koch, "3D printed dielectric rectangular waveguides, splitters and couplers for 120 GHz," *Opt. Exp.*, vol. 24, no. 25, p. 28968, Dec. 2016.
[54] D. Jahn, M. Weidenbach, J. Lehr, L. Becker, F. Beltrán-Mejía, S. F. Busch, J. C. Balzer, and M. Koch, "3D printed terahertz focusing grating couplers," *J. Infr., Millim., THz Waves*, vol. 38, no. 6, pp. 708–716, Jun. 2017.
[55] J. Ma, M. Weidenbach, R. Guo, M. Koch, and D. M. Mittleman, "Communications with THz waves: Switching data between two waveguides," *J. Infr., Millim., THz Waves*, vol. 38, no. 11, pp. 1316–1320, Nov. 2017.
[56] L. Jiu-Sheng, L. Han, and Z. Le, "Compact four-channel terahertz demultiplexer based on directional coupling photonic crystal," *Opt. Commun.*, vol. 350, pp. 248–251, Sep. 2015.
[57] W. Pan, X. Zhang, Y. Ma, Z. Zhang, X. Wang, T. Shen, Y. Li, and L. Yang, "A terahertz demultiplexer based on metamaterials applied to terahertz communication systems," *Prog. Electromagn. Res. Lett.*, vol. 97, pp. 13–19, 2021.
[58] G. Yan, A. Markov, Y. Chinifooroshan, S. M. Tripathi, W. J. Bock, and M. Skorobogatiy, "Low-loss terahertz waveguide Bragg grating using a two-wire waveguide and a paper grating," *Opt. Lett.*, vol. 38, no. 16, p. 3089, Aug. 2013.
[59] J. Yuan, T. Ning, H. Li, L. Pei, J. Li, J. Zheng, and L. Wan, "Terahertz filters based on subwavelength polymer waveguide," *Results Phys.*, vol. 13, Jun. 2019, Art. no. 102198.
[60] M. Burla, L. R. Cortés, M. Li, X. Wang, L. Chrostowski, and J. Azaña, "Integrated waveguide Bragg gratings for microwave photonics signal processing," *Opt. Exp.*, vol. 21, no. 21, p. 25120, Oct. 2013.
[61] M. A. Butt, N. L. Kazanskiy, and S. N. Khonina, "Advances in waveguide Bragg grating structures, platforms, and applications: An up-to-date appraisal," *Biosensors*, vol. 12, no. 7, p. 497, Jul. 2022.
[62] M.-C. Oh, H.-J. Lee, M.-H. Lee, J.-H. Ahn, S. G. Han, and H.-G. Kim, "Tunable wavelength filters with Bragg gratings in polymer waveguides," *Appl. Phys. Lett.*, vol. 73, no. 18, pp. 2543–2545, Nov. 1998.

BABAK YAHYAPOUR received the B.Sc. degree in physics from Urmia University, Urmia, Iran, in 2017, and the M.Sc. degree in photonics-electronics from Tabriz University, Tabriz, Iran, in 2019. He is currently pursuing the M.Sc. degree, under the supervision of Prof. Maksim Skorobogatiy. He is a Canada Research Chair Tier 1 in ubiquitous terahertz photonics. His research interests include THz circuits and THz communications.

FRÉDÉRIC MARCOTTE received the B.Eng. degree in engineering physics from Université Laval, Québec City, Canada, in 2023. He is currently pursuing the M.Sc. degree in electrical engineering under the supervision of Prof. Wei Shi. He is a Canada Research Chair in silicon photonics. His research interests include integrated photonic systems and optical communications.

ROYA GACHILOO received the B.Sc. degree in solid state physics from Kharazmi University, Tehran, Iran, in 2014, and the M.Sc. degree in photonics from Shahid Beheshti University, Tehran, in 2018. She is currently pursuing the M.Eng. degree in engineering physics with the Polytechnique Montréal, Montreal, QC, Canada, under the supervision of Prof. Maksim Skorobogatiy. Her research interests include the development and characterization of polymer fibers for terahertz communication and THz continuous wave spectroscopy.

MAKSIM SKOROBOGATIY (Senior Member, IEEE) received the M.Sc. degree in electrical engineering and computer science and the Ph.D. degree in physics from MIT, in 2000 and 2001, respectively. He was with MIT spin-off OmniGuide Inc., where he was involved in the development of hollow-core fibers for guidance of high-power mid-IR laser beams. He has been a Professor of engineering physics with the Polytechnique Montréal, since 2003. In 2017, he was an Elected Fellow of the Optical Society of America for his pioneering contributions to the development of micro-structured and photonic crystal multi-material fibers and their applications to light delivery, sensing, smart textiles, and arts. That same year, he was also promoted to a Senior Member of IEEE for his contribution to engineering and applied research. He was awarded the Tier 2 Canada Research Chair in Micro and Nano Photonics, in 2005 and 2010, while in 2016, he was awarded the Tier 1 Canada Research Chair in Ubiquitous THz Photonics. The support from Canada Research Chairs Program allowed him to pursue many high-risk exploratory projects in guided optics, smart materials, and recently THz photonics, which have resulted in significant contributions in these booming research fields. In 2012, he was awarded the rank of a Professional Engineer by the Order of Engineers of Quebec, Canada.